HYDRODYNAMICS AND RADIATION FROM COLLIDING PULSAR AND STELLAR WINDS IN A HIGH-MASS BINARY SYSTEM*

Gabriel Torralba Paz

Institute of Nuclear Physics Polish Academy of Sciences, 31-342 Kraków, Poland

Received 29 April 2022, accepted 4 May 2022, published online 9 September 2022

In this work, we discuss a semi-analytical model of the shocked wind of a pulsar embedded in a non-shocked wind of a massive star in the context of a high-mass binary system. Both winds collide at scales of the binary system, producing a contact discontinuity that creates shocked flows that go away from the system and are affected by the orbital motion. The shocked wind is made of charged particles and is assumed to be a relativistic, adiabatic, and ideal fluid. Under these assumptions, we compute the hydrodynamics of the wind as well as the non-thermal radiation emitted by the accelerated particles within the plasma in the region close to the binary system. Using this model, we predict the observed luminosity curves along the orbit that give us information about the inclination of the system, non-thermal processes, and the properties of both the massive star and the pulsar.

DOI:10.5506/APhysPolBSupp.15.3-A21

1. Introduction

X-ray binaries consist of a compact object (a black hole or a pulsar) and a massive star. In the case the system contains a pulsar, both components have powerful winds that interact with each other [1]. In the region where the winds collide, a discontinuity is created [2] and the winds are strongly slowed down, creating shocks that propagate through the pulsar wind (shocked wind), while the stellar wind surrounds the pulsar wind. The shocked wind is affected by the pulsar's orbital motion which causes a bending of the wind's trajectory into a spiral [3]. The plasma flows consist of mostly electrons and positrons [4], and can be treated as ideal, relativistic, and adiabatic fluids that follow the relativistic hydrodynamics (HD) equations [5]. In the shocks that are formed, particles can be accelerated to

* Presented at the 28$^{\text{th}}$ Cracow Epiphany Conference on *Recent Advances in Astroparticle Physics*, Cracow, Poland, 10–14 January, 2022. Originally presented at the University of Barcelona as a Master's Thesis.

ultra-relativistic energies and thus produce emission of non-thermal radiation from radio up to very high photon energies [6] in different non-thermal mechanisms such as Inverse Compton scattering [7] or synchrotron emission [8]. In this work, we extend the semi-analytical model developed in [3] to study the hydrodynamic and radiative consequences of an X-ray binary system containing a pulsar. Our model finds application in systems such as PSR B1259-63 [9] and PSR J2032+4127 [10] that contain very massive stars and pulsars albeit on elliptical orbits.

2. Dynamics of the shocked pulsar wind

We consider a pulsar in a circular orbit with radius D around a massive star located in the centre of the reference system (see Fig. 1). The physical parameters of the system are defined in Table 1. At the contact discontinuity (CD), the stellar and pulsar winds pressures are equal, and the apex of the CD is located at a distance $r_{\rm apex}$ from the star [11].

Table 1. Parameters of an X-ray binary system used in this work.

	Parameter	Symbol	Value
Star	luminosity	$L_\star$	$3 \times 10^{38}\,{\rm erg\,s^{-1}}$
	radius	$R_\star$	$10\,R_\odot$
	mass-loss rate	$\dot{M}_{\rm w}$	$3 \times 10^{-7}\,M_\odot\,{\rm yr^{-1}}$
	stellar wind speed	$v_{\rm w,r}$	$3 \times 10^{8}\,{\rm cm\,s^{-1}}$
Pulsar	pulsar luminosity	$L_{\rm P}$	$3 \times 10^{36}\,{\rm erg\,s^{-1}}$
	electron energy	E	0.01 erg
	mass-load rate factor	ε	0.8–1.0
System	orbital distance	D	$3 \times 10^{12}\,{\rm cm}$
	orbital period	T	5 days
	inclination	i	$0°, 30°, 60°, 90°$

The shocked wind has approximately a conical shape with a half-opening angle, θ, that depends on the pulsar–star wind momentum rate ratio η [12]

$$\theta = 28.6° \left(4 - \eta^{2/5}\right) \eta^{1/3}\,, \qquad \eta = \frac{L_{\rm P}}{\dot{M}_{\rm w} v_{\rm w,r} c}\,. \tag{1}$$

All calculations are done in the co-rotating frame of reference (RF) with the pulsar located at $r = (D, 0)$. We divide the shocked wind into two regions: the inner and the outer regions. In the inner region, the shocked wind starts at $r_{\rm apex}$ and flows in the x-direction away from the massive star.

The shocked wind ram pressure is strong enough, therefore, we can assume a 1D trajectory. The inner region will end at a distance $r_{\rm Cor}$ from the pulsar, where the shocked wind ram pressure is equal to the non-shocked stellar wind ram pressure due to the Coriolis force [13]

$$\frac{L_{\rm P}}{4\pi c r_{\rm Cor}^2} = \frac{\rho_{\rm w}(D)}{(1+r_{\rm Cor}/D)^2}\left(\frac{4\pi}{T}\right)^2 r_{\rm Cor}^2\,, \tag{2}$$

where $\rho_{\rm w}(r) = \dot{M}_{\rm w}/4\pi r^2 v_{\rm w,r}$ is the stellar wind density at a distance r from the star. The outer region starts right after the inner region. Note that after a quarter or half a turn of the wind spiral trajectory, this simplified description breaks down due to the assumptions made (see Section 3).

The trajectory is divided into N segments of length $\mathrm{d}l$ and variable radii R (see Fig. 1). For simplicity, we assume that both the stellar and pulsar winds are well separated with only a slight degree of mixing. In the inner region, the trajectory is simply $\boldsymbol{r}_{i+1} = \boldsymbol{r}_i + \mathrm{d}l\,\hat{x}$. In the outer region, the Coriolis force bends the trajectory

$$\boldsymbol{F}_{\rm w} = \rho_{\rm w} v_{\rm w}^2 S\,,\hat{\boldsymbol{v}}_{\rm w}\,, \tag{3}$$

where $\hat{\boldsymbol{v}}_{\rm w}$ is the stellar wind velocity in the co-rotating RF ($\mathrm{v}_{\rm w}^2 = v_{\rm w,r}^2 + \omega^2 r^2$), $S = 2R\mathrm{d}l\sin\alpha$, and α is the angle between the direction of the segment and $\hat{\boldsymbol{v}}_{\rm w}$. We assume no momentum exchange between winds and thus the fluid motions are ruled only by HD conservation laws. Finally, the dynamics are computed as

$$\dot{\boldsymbol{P}}_{i+1} = \dot{\boldsymbol{P}}_i + \boldsymbol{F}_{\rm w}\,, \qquad \boldsymbol{r}_{i+1} = \boldsymbol{r}_i + \mathrm{d}l\dot{\boldsymbol{P}}_{i+1}\,. \tag{4}$$

3. Hydrodynamics

All HD variables are computed in the RF fluid. We assume that the energy in the magnetic field is negligible and that the fluid does not exchange heat with the environment. The shocked wind fulfils the relativistic HD conservation equations and the adiabatic equation of state with adiabatic index $\hat{\gamma} = 4/3$, and an initial supersonic fluid velocity $v_0 = c/\sqrt{3}$.

The inner region [12] shows that for small values of the shocked wind Lorentz factor, γ, and close to the binary system, γ increases approximately linearly with distance. Note that in this region, the half-opening angle is not constant compared to the outer region (see Section 5.1). In the outer region, γ and the specific enthalpy h are large enough, therefore, we can consider an ultra-relativistic fluid. However, since γ decreases along the trajectory in the outer region (see Fig. 2, right), we stop the model at $\gamma = 2$ to ensure that the ultra-relativistic fluid approximation is valid. The boundaries between the

shocked pulsar and stellar winds may become unstable at far distances from the binary and mixing may occur due to plasma instabilities. To model this, we assume a non-constant mass load rate, $\dot{M}$, that increases with distance and so it affects the energy per particle $h\gamma$

$$\dot{M}(r) = \dot{M}_0 \left(\frac{r}{D + r_{\rm Cor}} \right)^{\varepsilon}, \qquad h\gamma = h_0 \gamma_{\rm P} \left(\frac{r}{D + r_{\rm Cor}} \right)^{-\varepsilon}, \tag{5}$$

where $\dot{M}_0$, h_0, and $\gamma_{\rm P}$ are measured prior to the winds collision, at $r = r_{\rm apex}$, and ε controls how fast the mass rate increases. This effect of mixing slows down the shocked wind and may lead to a reduction of the emitted luminosity.

4. Radiation mechanism

We assume a simple model for the emitted radiation which includes Doppler boosting effects. Primed quantities are computed in the RF fluid, whereas unprimed quantities are computed in the RF observer. The observer luminosity is calculated as the sum of the luminosity of each segment [14]

$$\mathrm{d}L = \frac{\delta^3}{\gamma} \mathrm{d}L', \qquad L = \sum_{i=1}^{N} \mathrm{d}L, \tag{6}$$

where $\delta = [\gamma (1 - \beta \cos \varphi)]^{-1}$ is the Doppler boosting factor, $\beta = v/c$, and φ is the angle between the direction of the segment and the direction of the observer. In this work, we exclusively consider the Inverse Compton (IC) emission and we neglect the synchrotron emission processes that may be important only very close to the pulsar.

The cooling time in the IC emission in the Thomson regime is

$$t'_{\rm cool} = \frac{E'}{\left| \dot{E}' \right|}, \qquad \dot{E}' = \frac{4}{3} \frac{\sigma_{\rm T} c}{(m_{\rm e} c^2)^2} u'_{\star} E'^2 \approx 0.039 u'_{\star} E'^2, \tag{7}$$

where $\sigma_{\rm T}$ is the Thomson cross section, $m_{\rm e}$ is the mass of the electron, $u'_{\star}$ is the energy density of the radiation of the massive star, and E' is the total energy of an emitting particle. To compute E', we use calculations made by [15] that give

$$E' = \left(\frac{\delta_{*,\rm seg}}{\delta} \right) E, \tag{8}$$

where $\delta_{*,\rm seg} = [\gamma (1 - \beta \cos \xi)]^{-1}$ is the Doppler boosting factor at a trajectory segment, ξ is the angle between the direction of that segment and the

direction from the star to the segment, and E is the electron energy in the RF observer, which is assumed mono-energetic. The energy density of the radiation is just $u'_\star = u_\star/\delta^2_{*,\mathrm{seg}}$ with $u_\star \simeq L_\star/4\pi r^2 c$.

Finally, the luminosity per segment in the RF fluid is

$$\mathrm{d}L' = 0.1\,\mathrm{d}V'\,(1-\cos\psi)\,\frac{u}{t'_{\mathrm{cool}}}\,, \tag{9}$$

where $\mathrm{d}V' = \gamma \mathrm{d}V$ is the volume of the segment in the RF fluid and u is the internal energy of the fluid that can be computed with the assumption of an adiabatic gas, $u = P/(\hat{\gamma}-1) = 3P$. Here, we also assume that about 10% of the internal energy of the plasma is converted into the form of non-thermal radiation in the IC process.

5. Results

The results are presented for $\varepsilon = 1$, except in Section 5.4. We define the orbital phase ϕ as the angle between the direction to the observer and the star–pulsar distance. In the co-rotating RF, ϕ grows in the opposite direction to the motion of the pulsar.

5.1. 2D dynamics

In figure 1, we show the trajectory of the shocked pulsar wind starting at $r = r_{\mathrm{apex}}$. Note that the shocked wind does not start with a conical shape, but acquires it as it slowly bends towards the outer region. Using our model, we can explain with precision the shocked wind at distances on the scale of the system. However, at larger distances, our description may not be valid, as due to the ultra-relativistic fluid approximation this breaks down.

5.2. Hydrodynamic evolution

Figure 2 (left) shows the evolution of the specific enthalpy, pressure, and density of the shocked wind along its trajectory. The vertical black dashed line separates the inner and the outer regions. The three fluid quantities have a very similar evolution along the trajectory, with a steep decrease in the inner region, an abrupt change between the inner and the outer regions, and a slow decline in the outer region. The Lorentz factor of the wind (Fig. 2, right), instead, increases linearly in the inner region (see Section 3), but decreases suddenly in the outer region due to the increasing mass load rate $\dot{M}$ of the shocked wind.

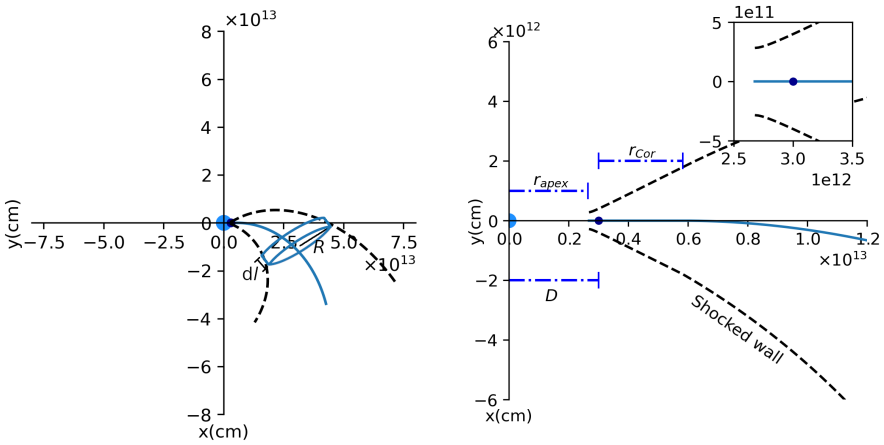

Fig. 1. (Colour on-line) The trajectory of the pulsar wind (left) and a zoom-in at the scale of the system (right). The big light-blue dot is the massive star, the dark blue dot is the pulsar, the wind trajectory is marked with the solid blue curve, and black dashed lines mark the boundaries of the shocked wind. A cylindrical segment with height dl and variable radius R used for calculations is presented in the left panel.

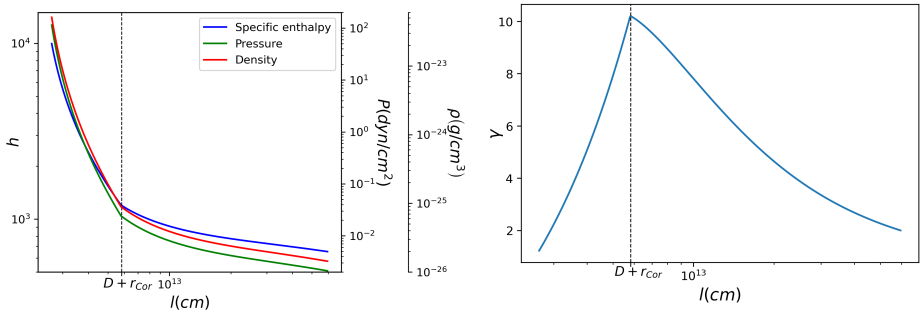

Fig. 2. (Colour on-line) The evolution of the hydrodynamical parameters of the shocked wind (left) and the wind Lorentz factor (right) along the shocked wind trajectory. The black dashed vertical line separates the inner and the outer regions.

5.3. Radiation consequences

Figure 3 (left) shows the Doppler boosting factor along the shocked wind trajectory for different orbital phases and an orbit inclination of $i = 90°$. Segments that have the same direction as the observer give the maximum value of δ.

Figure 3 (right) shows the total luminosity for a full orbital phase and different inclinations. With a maximum variation of $\sim 630\%$, the maximum is found around $\phi \approx \pi/3$, where most of the segments have a high Doppler boosting and provide a high luminosity per segment. On the contrary, for

$\phi \approx \pi$, we find the minimum of the luminosity, as most segments point away from the direction of the observer. As the orbit inclination decreases, the phase dependence becomes less significant and it disappears at $i = 0°$.

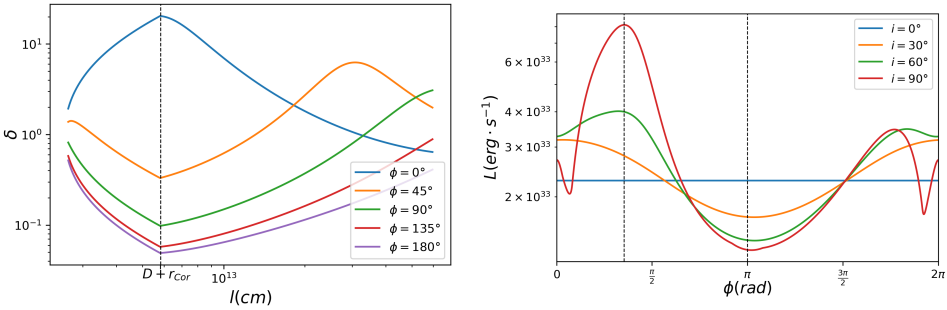

Fig. 3. The Doppler boosting factor along the trajectory (left) for $i = 90°$ and the luminosity for the inverse Compton scattering for a full orbital phase (right).

5.4. The ε parameter

Figure 4 (left) shows the Lorentz factor along the trajectory for different values of the mixing parameter ε. With a higher ε, more mass is loaded into the shocked wind and γ drops fast with a distance. For lower ε, the Lorentz factor decreases slower and the trajectory of the shocked wind is longer.

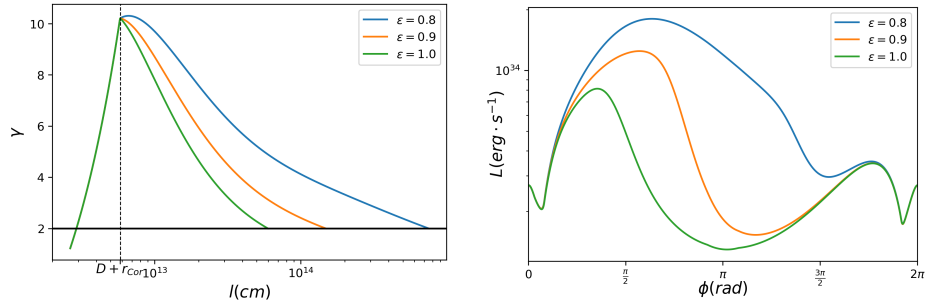

Fig. 4. The Lorentz factor along the trajectory (left) and the luminosity curve for a full orbital phase and $i = 90°$ for different values of ε (right).

Figure 4 (right) shows luminosity curves for three values of ε. For low values of the orbital phase, $\phi \approx 0$, the behaviour is similar for all ε. At higher ϕ, the observed luminosity increases significantly for $\varepsilon < 1$ due to the increased wind Lorentz factor and there is a much wider range of ϕ for which segments are facing the observer. The maximum luminosity variation now reaches $\sim 1400\%$ for $\varepsilon = 0.8$, a factor of more than 2 compared to $\varepsilon = 1$. This may have clear observational consequences.

6. Summary and conclusions

In this work, we used a semi-analytical model of the shocked wind in an X-ray binary system consisting of a massive star and a pulsar. The trajectory of the pulsar wind is affected by the orbital motion of the pulsar around the massive star and by the plasma mixing at the boundaries between the stellar and pulsar winds. The interaction between the winds creates shocks that propagate through the pulsar wind and accelerate particles, producing radiation. In this work, we focus on IC scattering. Our model describes the evolution of HD wind parameters and predicts luminosity curves for different inclinations of the orbit and different values of ε that controls plasma mixing. We find a maximum variation of $\sim 1400\%$ for an orbit inclination of $i = 90°$ and $\varepsilon = 0.8$. Our hydrodynamic treatment is accurate due to the assumed low density. However, as the pressure decreases, the stellar wind may destabilise the shocked wind and our proposed model might not be able to predict accurately the shocked wind behaviour. Despite this, our results can be applied to X-ray binaries such as PSR B1259-63 and PSR J2032+4127 that have physical parameters compatible with those used here.

I want to thank my advisor during my master thesis, Valentí Bosch i Ramon, for supervising and counselling me.

REFERENCES

[1] X. Paredes-Fortuny, V. Bosch-Ramon, M. Perucho, M. Ribó, «Simulations of an inhomogeneous stellar wind interacting with a pulsar wind in a binary system», *Astron. Astrophys.* **574**, A77 (2015).

[2] R.T. Emmering, R.A. Chevalier, «Shocked relativistic magnetohydrodynamic flows with application to pulsar winds», *Astrophys. J.* **321**, 334 (1987).

[3] E. Molina, V. Bosch-Ramon, «A dynamical and radiation semi-analytical model of pulsar-star colliding winds along the orbit: Application to LS 5039», *Astron. Astrophys.* **641**, A84 (2020).

[4] G. La Mura *et al.*, «Relativistic plasmas in AGN jets», *Eur. Phys. J. D* **71**, 95 (2017).

[5] V. Bosch-Ramon, M.V. Barkov, M. Perucho, «Orbital evolution of colliding star and pulsar winds in 2D and 3D: effects of dimensionality, EoS, resolution, and grid size», *Astron. Astrophys.* **577**, A89 (2015).

[6] L. Maraschi, A. Treves, «A model for LSI 61 303», *Mon. Not. R. Astron. Soc.* **194**, 1P (1981).

[7] L. Ball, J. Kirk, «Probing pulsar winds using inverse Compton scattering», *Astropart. Phys.* **12**, 335 (2000).

[8] D. Kandel, R.W. Romani, H. An, «The Synchrotron Emission Pattern of Intrabinary Shocks», *Astrophys. J.* **879**, 73 (2019).

[9] F. Aharonian *et al.*, «Discovery of the binary pulsar PSR B1259-63 in very-high-energy gamma rays around periastron with HESS», *Astron. Astrophys.* **442**, 1 (2005).

[10] A.U. Abeysekara *et al.*, «Periastron Observations of TeV Gamma-Ray Emission from a Binary System with a 50-year Period», *Astrophys. J. Lett.* **867**, L19 (2018).

[11] D. Eichler, V. Usov, «Particle acceleration and nonthermal radio emission in binaries of early-type stars», *Astrophys. J.* **402**, 271 (1993).

[12] S.V. Bogovalov *et al.*, «Modelling interaction of relativistic and non-relativistic winds in binary system PSR B1259-63/SS2883 — I. Hydrodynamical limit», *Mon. Not. R. Astron. Soc.* **387**, 63 (2008).

[13] V. Bosch-Ramon, M.V. Barkov, «Large-scale flow dynamics and radiation in pulsar γ-ray binaries», *Astron. Astrophys.* **535**, A20 (2011).

[14] M. Sikora, G. Madejski, R. Moderski, J. Poutanen, «Learning about Active Galactic Nucleus Jets from Spectral Properties of Blazars», *Astrophys. J.* **484**, 108 (1997).

[15] C.D. Dermer, R. Schlickeiser, «Transformation Properties of External Radiation Fields, Energy-Loss Rates and Scattered Spectra, and a Model for Blazar Variability», *Astrophys. J.* **575**, 667 (2002).